Hindawi
Quantum Engineering
Volume 2023, Article ID 8993363, 11 pages
https://doi.org/10.1155/2023/8993363

Research Article

Continuous-Variable Pairwise Entanglement Based on Optoelectromechanical System

Qizhi Cai,[1] **Jinkun Liao**,[2] **and Qiang Zhou**[1]

[1]*Institute of Fundamental and Frontier Sciences, University of Electronic Science and Technology of China, Chengdu, Sichuan, China*
[2]*School of Optoelectronic Science and Engineering, University of Electronic Science and Technology of China, Chengdu, Sichuan, China*

Correspondence should be addressed to Qiang Zhou; zhouqiang@uestc.edu.cn

Received 20 March 2023; Revised 7 September 2023; Accepted 6 October 2023; Published 31 October 2023

Academic Editor: YuBo Sheng

We show how to generate stationary continuous-variable pairwise entanglement between microwave modes in a hybrid optoelectromechanical system, which consists of a single Fabry–Pérot cavity, a parallel-plate capacitor with a moving element as the mechanical resonator, and several pairs of microwave cavities. The optical mode and mechanical resonator are coupled via radiation pressure; meanwhile, several pairs of the microwave mode and mechanical resonator are capacitively coupled. Under an experimentally reachable parameter regime, we show the influence of different key parameters on pairwise entanglement and find that it is also robust against temperature. Our model and results are expected to provide a new perspective on quantum networks with increasingly large scales, quantum internet with multiple local users, and multiport microwave quantum illumination radar.

1. Introduction

The quantum network lies at the heart of currently developed quantum technologies [1–15]. It would become increasingly mature when it became possible to integrate various modules into a single hybrid device and build networks based on these hybrid devices. As it is foreseeable that an ideal future quantum network may have multiple local users simultaneously, it is necessary to generate quantum entanglement between local units or nodes that are usually operating at microwave range and enable this kind of multipartite node to interface with other remote nodes.

Pairwise measures of correlations and mutual information are widely used to characterize the interactions within classical networks, which are key ingredients of widespread techniques such as principal component analysis and functional networks for their greatly simplified descriptions of complex systems [16]. In particular, the concept of pairwise is also utilized to study the properties of multiqubit entanglement generation [17].

Inspired by pairwise networks in the discrete-variable regime for quantum many-body systems [18–20], in this work, we propose a scheme to generate pairwise entanglement between microwave mode in a continuous-variable (CV) regime based on an optoelectromechanical system [21–40], which has the potential to be utilized in quantum technologies with large scale in the CV regime. For instance, this model can be used in multiuser quantum networks, where local users can share the microwave pairwise entanglement locally, and the optical part is capable of connecting a remote quantum "base station" with well-developed fiber optic technology [1–3]. Moreover, such pairwise entanglement is also expected to be useful in short-range quantum illumination radar [39–41] for all-around noninvasive biomedical scanning due to multipair entangled microwave modes corresponding to multiple parallel data received and other applications in the CV regime [42–49].

This paper is organized as follows. Section 2 shows the physical model of the system, with its quantum Langevin equations for describing the dynamics of the system and

their linearization. In Section 3, we will derive the correlation matrix of the quantum fluctuations of the system in order to obtain the logarithmic negativity, which is considered the entanglement measure in this work. As the microwave-to-optical conversion mediated by a mechanical resonator is well investigated both from a theoretical and experimental perspective [29–31], in this work, we mainly focus on the pairwise entanglement between microwave modes. Therefore, we analyze the influence of some key parameters on CV microwave pairwise entanglement in Section 4, and Section 5 is for the conclusion.

2. Model

We consider a hybrid optoelectromechanical system containing $n + 2$ units, as shown in Figure 1, where a represents Fabry–Pérot optical cavity (OC) with resonant frequency, ω_c, m indicates mechanical resonator with resonant frequency ω_m, and b_j ($j = 1, 2, ..., n$, n is even) corresponds to the microwave cavity (MC) with resonant frequency ω_{wj}. In this model, two MCs can be regarded as a pair with suitable parameter settings, as the results part will discuss; each MC is capacitively coupled with the mechanical resonator simultaneously, while, the mechanical resonator is coupled with the OC via radiation pressure. The Hamiltonian of the system reads [24–26]

$$H = \hbar\omega_c a^\dagger a + \sum_{j=1}^{n} \hbar\omega_{wj} b_j^\dagger b_j + \frac{\hbar\omega_m}{2}\left(p^2 + q^2\right) - \sum_{j=1}^{n} \frac{\hbar G_{0wj}}{2} q b_j^\dagger b_j - \hbar G_{0c} q a^\dagger a$$
$$- \sum_{j=1}^{n} i\hbar E_{wj}\left(e^{i\omega_{0wj}t} - e^{-i\omega_{0wj}t}\right)\left(b + b^\dagger\right) + i\hbar E_c\left(a^\dagger e^{-i\omega_{0c}t} a e^{i\omega_{0c}t}\right), \tag{1}$$

where a ($a^\dagger$) and b ($b^\dagger$) are the annihilation (creation) operator for OC and MCs, q and p are the dimensionless position and momentum operators for mechanical resonator, satisfying $[a, a^\dagger] = 1$, $[b_j, b_j^\dagger] = 1$, and $[q, p] = i$. $G_{0c} = (\omega_c/l)\sqrt{\hbar/m_c\omega_m}$ is the optomechanical vacuum coupling with l as the length of the OC and m_c as the effective mass of mechanical resonator interacting with the OC. The optical driving strength is $E_c = \sqrt{2P_c\kappa_c/\hbar\omega_{0c}}$ with P_c as the driving power and κ_c as damping rates of OC. The microwave-driving strength for cavity j is $E_{wj} = \sqrt{2P_{wj}\kappa_{wj}/\hbar\omega_{0wj}}$ with P_{wj} as the driving power and κ_{wj} as damping rates for j th MC. The electromechanical vacuum coupling of j th MC is given by [28]

$$G_{0wj} = -\beta_j \frac{\omega_{wj}}{2C_{\mathrm{mod},j}} \frac{dC_{\mathrm{mod},j}}{dx_j} x_{zpf,j}, \tag{2}$$

where $C_{\mathrm{mod},j}$ is the modulated capacitance, $C_{\mathrm{tot},j}$ is the total circuit capacitance, $\beta_j = C_{\mathrm{mod},j}/C_{\mathrm{tot},j}$ is the capacitance ratio, x_j is the amplitude coordinate, $x_{zpf,j} = \sqrt{\hbar/2m_{wj}\omega_m}$ is the zero-point fluctuations, and m_{wj} is the effective mass of the mechanical resonator interacting with j th MC.

In the frame rotating at $H_0 = \hbar\omega_{0c} a^\dagger a + \sum_{j=1}^{n} \hbar\omega_{0wj} b_j^\dagger b_j$ and neglect fast oscillating terms at $\pm 2\omega_{0c}$, $\pm 2\omega_{0wj}$, the reduced Hamiltonian becomes

$$H = \hbar\Delta_{0c} a^\dagger a + \sum_{j=1}^{n} \hbar\Delta_{0wj} b_j^\dagger b_j + \frac{\hbar\omega_m}{2}\left(p^2 + q^2\right) - \sum_{j=1}^{n} \frac{\hbar G_{0wj}}{2} q b_j^\dagger b_j - \hbar G_{0c} q a^\dagger a$$
$$- \sum_{j=1}^{n} i\hbar E_{wj}\left(b - b^\dagger\right) + i\hbar E_c\left(a^\dagger - a\right), \tag{3}$$

in which $\Delta_{0c} = \omega_c - \omega_{0c}$ and $\Delta_{0wj} = \omega_{wj} - \omega_{0wj}$ with ω_{0wj} and ω_{0c} are the driving frequencies of MCs and OC, respectively. By using the Heisenberg equations, the quantum Langevin equations (QLEs) describing the system dynamics read

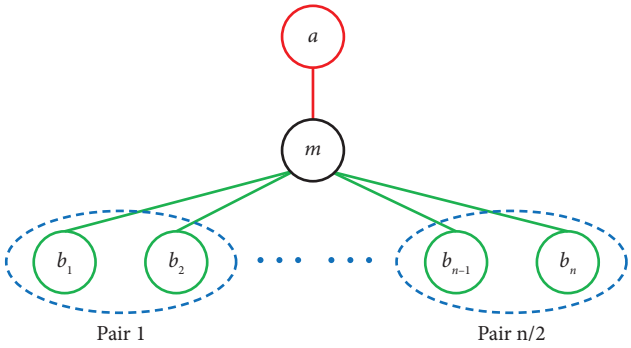

FIGURE 1: Simple sketch for the hybrid optoelectromechanical system. a is for the optical cavity. m is for the mechanical resonator, and b_j is for the multipair microwave cavities.

$$\begin{aligned}
\dot{q} &= \omega_m p,\\
\dot{p} &= -\omega_m q - \kappa_m p + G_{0c} a^\dagger a + \sum_{j=1}^{n} G_{0wj} b_j^\dagger b_j + \xi,\\
\dot{a} &= -\left(i\Delta_{0c} + \kappa_c\right) a + iG_{0c} q a + E_c + \sqrt{2\kappa_c}\, a^{\text{in}},\\
\dot{b}_j &= -\left(i\Delta_{0wj} + \kappa_{wj}\right) b_j + iG_{0wj} q b_j + E_{wj} + \sqrt{2\kappa_{wj}}\, b^{\text{in},j},
\end{aligned} \tag{4}$$

where κ_m, κ_a, and κ_{wj} are damping rates of the mechanical resonator, OCs, and MCs, respectively. $\xi(t)$ is the quantum Brownian noise acting on the mechanical resonator, with the correlation function [50]

$$\frac{\langle \xi(t)\xi(t') + \xi(t')\xi(t)\rangle}{2} \approx \kappa_m\left(2\overline{n}_m + 1\right)\delta\left(t - t'\right), \tag{5}$$

in which we have assumed that $Q_m = \omega_m/\kappa_m \gg 1$, which is valid in our model, $\overline{n}_m = 1/[\exp\ (\hbar\omega_m/k_B T) - 1]$ is the thermal excitation, k_B is the Boltzmann constant, and T is the environmental temperature. The optical and microwave input noises are given by a^{in} and $b^{\text{in},j}$, which can be considered as zero-mean Gaussian, satisfying the following correlation functions [51]:

$$\begin{aligned}
\langle a^{\text{in}}(t) a^{\text{in},\dagger}(t')\rangle &= \left[N(\omega_c) + 1\right]\delta(t - t'),\\
\langle a^{\text{in},\dagger}(t) a^{\text{in}}(t')\rangle &= N(\omega_c)\delta(t - t'),\\
\langle b^{\text{in},j}(t) b^{\text{in},j,\dagger}(t')\rangle &= \left[N\left(\omega_{wj}\right) + 1\right]\delta(t - t'),\\
\langle b^{\text{in},j,\dagger}(t) b^{\text{in},j}(t')\rangle &= N\left(\omega_{wj}\right)\delta(t - t'),
\end{aligned} \tag{6}$$

where $N(\omega_c) = 1/[\exp\ (\hbar\omega_c/k_B T) - 1]$ and $N(\omega_{wj}) = 1/[\exp\ (\hbar\omega_{wj}/k_B T) - 1]$ are the mean thermal numbers of optical and microwaves fields, respectively.

In our model, each MC and OC are driven intensely, which gives a large amplitude for all cavities $\langle O\rangle \gg 1$ $(O = a, b_j, q, p)$, which is valid in state-of-the-art technology. Under this condition, we can linearize the dynamic around the semiclassical points of each cavity, by writing all operators as $O = O_s + \delta O$, where we have neglected high-order fluctuation terms. Then, we can focus on the linearized dynamics of the system by inserting these approximations into equation (4). By setting the derivatives to zero, the fixed semiclassical points for each subsystem reads

$$\begin{aligned}
p_s &= 0,\\
q_s &= \frac{G_{0c}\left|\alpha_s\right|^2 + \sum_{j=1}^{n} G_{0wj}\left|\beta_{sj}\right|^2}{\omega_m},\\
\alpha_s &= \frac{E_c}{\kappa_c + i\Delta_c},\\
\beta_{sj} &= \frac{E_{wj}}{\kappa_{wj} + i\Delta_{wj}},
\end{aligned} \tag{7}$$

where $\Delta_c = \Delta_{0c} - G_{0c} q_s$ and $\Delta_{wj} = \Delta_{0wj} - G_{0wj} q_s$ are the effective detuning of the optical and microwave fields, respectively. The linear QLEs for quantum fluctuations are given by

$$\begin{aligned}
\delta\dot{q} &= \omega_m \delta p,\\
\delta\dot{p} &= -\omega_m \delta q - \kappa_m \delta p + G_{0c}\alpha_s\left(\delta a^\dagger + \delta a\right) + \sum_{j=1}^{n} G_{0wj}\beta_{sj}\left(\delta b_j^\dagger + \delta b_j\right) + \xi,\\
\delta\dot{a} &= -\left(\kappa_c + i\Delta_c\right)\delta a + iG_{0c}\alpha_s \delta q + \sqrt{2\kappa_c}\, a^{\text{in}},\\
\delta\dot{b}_j &= -\left(\kappa_{wj} + i\Delta_{wj}\right)\delta b_j + iG_{0wj}\beta_{sj}\delta q + \sqrt{2\kappa_{wj}}\, b^{\text{in},j},
\end{aligned} \tag{8}$$

where we have appropriately chosen phase references for all of the input optical and microwaves fields so that α_s and β_{sj} can be taken real and positive.

3. Correlation Matrix of the System and Quantification of CV Pairwise Entanglement

In order to obtain the correlation matrix that calculates stationary CV entanglement between pairwise microwave modes, we shall introduce the quadratures $\delta X_c = (\delta a + \delta a^\dagger)/\sqrt{2}$ and $\delta Y_c = (\delta a - \delta a^\dagger)/i\sqrt{2}$ for OC, $\delta X_{wj} = (\delta b + \delta b^\dagger)/\sqrt{2}$ and $\delta Y_{wj} = (\delta b - \delta b^\dagger)/i\sqrt{2}$ for MCs, $\delta X^{c,\mathrm{in}} = (\delta a^{\mathrm{in}} + \delta a^{\mathrm{in},\dagger})/\sqrt{2}$, $\delta Y^{c,\mathrm{in}} = (\delta a^{\mathrm{in}} - \delta a^{\mathrm{in},\dagger})/i\sqrt{2}$, $\delta X^{wj,\mathrm{in}} = (\delta b^{\mathrm{in},j} + \delta b^{\mathrm{in},j,\dagger})/\sqrt{2}$, and $\delta Y^{wj,\mathrm{in}} = (\delta b^{\mathrm{in},j} - \delta b^{\mathrm{in},j,\dagger})/i\sqrt{2}$ for each corresponding noises, then the linear QLEs become

$$\begin{aligned}
\delta\dot{q} &= \omega_m \delta p,\\
\delta\dot{p} &= -\omega_m \delta q - \kappa_m \delta p + G_c \delta X_c + \sum_{j=1}^{n} G_{wj}\delta\widehat{X}_{wj} + \xi,\\
\delta\dot{X}_c &= -\kappa_c \delta X_c + \Delta_c \delta Y_c + \sqrt{2\kappa_c}X^{c,\mathrm{in}},\\
\delta\dot{Y}_c &= -\Delta_c \delta X_c - \kappa_c \delta Y_c + G_c \delta q + \sqrt{2\kappa_c}Y^{c,\mathrm{in}},\\
\delta\dot{X}_{wj} &= -\kappa_{wj}\delta X_{wj} + \Delta_{wj}\delta Y_{wj} + \sqrt{2\kappa_{wj}}X^{wj,\mathrm{in}},\\
\delta\dot{Y}_{wj} &= -\Delta_{wj}\delta X_{wj} - \kappa_{wj}\delta Y_{wj} + G_{wj}\delta q + \sqrt{2\kappa_{wj}}Y^{wj,\mathrm{in}},
\end{aligned} \tag{9}$$

where

$$\begin{aligned}
G_{wj} &= \sqrt{2}G_{0wj}\beta_{sj} = 2G_{0wj}\sqrt{\frac{P_{wj}\kappa_{wj}}{\hbar\omega_{0wj}\left(\kappa_{wj}^2 + \Delta_{wj}^2\right)}},\\
G_c &= \sqrt{2}G_{0c}\alpha_s = 2G_{0c}\sqrt{\frac{P_c\kappa_c}{\hbar\omega_c\left(\kappa_c^2 + \Delta_c^2\right)}},
\end{aligned} \tag{10}$$

are the effective the electromechanical and optomechanical couplings, respectively. Equation (10) can be rewritten in the form of

$$\dot{u}(t) = Au(t) + n(t), \tag{11}$$

where $u(t) = [\delta q, \delta p, \delta X_c, \delta Y_c, \delta X_{w1}, \delta Y_{w1}, ..., \delta X_{wn}, \delta Y_{wn}]^T$ (the notation T means matrix transpose) is a column vector with 2 n +4 dimensions, the same as the noise vector $n(t)$, and drift matrix A is a (2 n +4) × (2 n +4) square matrix, whose explicit expression is shown in Appendix A. As mentioned above, the dynamics describing the system are linear and the quantum noise terms in equation (12) are zero-mean Gaussian. So the steady state of the quantum fluctuations is a Gaussian state of n +2 modes, completely characterized by a (2 n +4) × (2 n +4) correlation matrix, which can be attained by solving the Lyapunov equation [52, 53]

$$\mathrm{AV} + \mathrm{VA}^T = -D, \tag{12}$$

where $D = \mathrm{Diag}[0, \kappa_m(2\overline{n}_m + 1), \kappa_c, \kappa_c, \kappa_{w1}(2N(\omega_{w1}) + 1), \kappa_{w1}(2N(\omega_{w1}) + 1), ., \kappa_{wn}(2N(\omega_{wn}) + 1), \kappa_{wn}(2N(\omega_{wn}) + 1)]$. As V is obtained, the logarithmic negativity or the measure of CV entanglement of interested bipartite systems can be obtained by tracing out the rows and columns of other subsystems. With this operation, the reduced 4 × 4 correlation matrix describing the interested bipartite pairwise subsystem is

$$V_{bi} = \begin{pmatrix} V_1 & V_3 \\ V_3^T & V_2 \end{pmatrix}, \tag{13}$$

and the entanglement between this pairwise modes is given by [54, 55]

$$E_N = \max\left[0, -\ln\ 2\eta^-\right], \tag{14}$$

where $\eta^- \equiv 2^{-1/2}\left[\Sigma(V_{bi}) - \sqrt{\Sigma(V_{bi})^2 - 4\det V_{bi}}\right]^{-1/2}$ and $\Sigma(V_{bi}) \equiv \det V_1 + \det V_2 - 2\det V_3$.

4. Results

As the microwave-to-optical conversion mediated by a mechanical resonator has been well investigated in recent years [29–31], in this section, we mainly focus on the CV pairwise entanglement between microwave modes. All results satisfy the Routh–Hurwitz criterion described in Appendix A unless specifically stated, which guarantees the steady state of the system. The parameter regime is a feasible extension over previous experimental works [23, 27, 28, 38] for the optical part, driving laser wavelength $\lambda_{0c} = 1550$ nm, damping rate $\kappa_c/2\pi = 2.8$ MHz, driving power $P_c = -68$ dBm, vacuum optomechanical coupling $G_{0c}/2\pi = 125$ kHz, and optical effective detuning $\Delta_c = 0.5\ \omega_m$. For mechanical resonator, resonant frequency $\omega_m/2\pi = 2.8$ MHz and damping rate $\kappa_m/2\pi = 10$ Hz. For the microwave part, the parameters of two MCs in each pair are almost the same except for effective detuning Δ_{wj} for satisfying the Routh–Hurwitz criterion. These two detunings are opposite $\Delta_{w1} = -\Delta_{w2}$, and every newly added microwave pair should follow this criterion. Under this condition, the other parameter between distinct microwave pairs can be different, which will not affect the stability of the system. For simplicity, we choose all microwave pairs with the same parameters except the resonant frequency of each MC at first. The parameters for MCs read: damping rates $\kappa_w/2\pi = 170$ kHz, input power $P_w = -68$ dBm, the vacuum electromechanical coupling $G_{0w} = [\omega_w/(2\pi \times 12.13)] \cdot 510$ kHz with capacitor gap $d \approx 30$ nm [27, 28] and the unit of ω_w is GHz. The effective microwave detunings are defined as $\Delta_w \equiv \Delta_{w1} = -\Delta_{w2} = \cdots = \Delta_{w(n-1)} = -\Delta_{wn}$. For each MC pair, the detunings of two MCs have the same absolute value but opposite signs. In the following, we label the MC resonant at 9 GHz with positive or negative detuning as 9+ or 9−. Other unmentioned parameters are shown below each figure.

In Figure 2, we mainly focus on the influence of the microwave pair number on the entanglement, so we make all MCs have the same resonance frequency at 9 GHz. In this case, there are four MCs with their detunings $\Delta_w \equiv \Delta_{w1} = -\Delta_{w2} = \Delta_{w3} = -\Delta_{w4}$, where MCs with detunings Δ_{w1} and Δ_{w2} are regarded as a pair, so does for Δ_{w3} and Δ_{w4}. For simplification of expression, we define Δ_{w1} and Δ_{w3} as the positive detuning and Δ_{w2} and Δ_{w4} as the negative

detuning in the MC pairs. We find that the entanglement only exists between two MCs whose detunings are opposite. Also, one can notice that these entanglement curves have a dip at the point $\Delta_w = 0$. This is because at this point all the microwave cavities are on-resonance, and the pair designation becomes arbitrary. Under this condition, two arbitrarily picked microwave cavities can get entangled. Back to pair number's influence on the pairwise entanglement, the pairwise entanglement declines as the MC pairs are added. It can be phenomenologically thought that, as the scale of the system increases, the correlation between the subsystems deceases. Under this kind of structural design and parameter setting, we can further explore the maximum network size where CV entanglement still exists or is useful. We find that the pairwise entanglement will not be zero but will approach zero when we add microwave pairs. So in theory, we can consider that, under this kind of structural design and parameter setting, one can continuously generate such pairwise entanglement in the system with a larger size as long as the experimental conditions allow.

Then, we turn to study the condition where various microwave pairs resonate at different frequency ranges. For simplicity, we choose the 3-pair system, in which the first MC pair resonates at 9 GHz, 37.5 GHz for the second, and 60 GHz for the third. In principle, modes with any resonant frequency in the microwave band can get entangled in our system, which is beneficial for fulfilling the requirements of broadband working in quantum networks and the Internet. From Figure 3, we can know that the higher the frequency of two microwave modes, the larger the entanglement between them can be achieved. It happens in part because higher-frequency microwave photon contains more energy, which leads to stronger robustness in the thermal noise environment. We also notice that the entanglement between 37.5+ and 60− is virtually the same compared with the trace of 37.5− and 60+, as it is for other pairs. The reason why there is a little asymmetry is because of the asymmetrical parameter settings, i.e., the frequencies of two entangled microwave modes are not identical.

Based on the two models described above, we further investigate the relation between pairwise entanglement and temperature. As shown in Figure 4(a), we find that the pairwise entanglement still survives above 100 mK in a system containing 10 MC pairs. The entanglement in more scalable systems shows lower resistance in the thermal environment. In Figures 4(b) and 4(c), we find that the entanglement between higher-frequency microwave modes is larger and can show stronger thermal robustness. Both of them correspond to the above statement.

From Figure 3, we have already known that the detuning of two entangled microwave modes in such a pairwise system should have opposite signs. Next, we study the influence of the absolute value of detuning on such entanglement. From Figure 4(d), we find that the pairwise entanglement merely exists between two MCs whose detunings have the same absolute values and opposite signs. As shown in Figure 4(e), an enlarged plot of Figure 4(d) around the zero-detuning point, the entanglement of other combinations only appears near the zero-detuning point, where all MCs are truly identical, so that the pair designation becomes arbitrary, and this is why all traces will intersect at a zero-detuning point. In Figure 4(f), the 2-pair system described in Figure 2 with identical absolute value detunings, we find that the entanglement will not exist in a wide detuning range between two MCs with the same absolute value detunings and same signs. Therefore, we can conclude that the detunings of two entangled MCs should have opposite signs and identical absolute values when wide-range detuned. Furthermore, using this feature, we can make an entanglement switch that can turn on or off the entanglement between MCs by changing the detunings of each MC.

In real experimental implementations, there will always be some variation in the parameters. So we analyze the impact of detuning deviation of a single MC $\Delta_d = \Delta_{w1} - \Delta_w$ on pairwise entanglement in Figure 5, this analysis method is also applicable to multipair MC deviating conditions. The model studied is the 2-pair system described in Figure 2, except that a detuning deviation Δ_d is exerted on one MC named $\widetilde{9}+$. From Figure 5(a), if $\Delta_d = 2\pi \times 50$ kHz, the system will be unstable near the zero-detuning region, which makes the pairwise entanglement vanish, while the pairwise entanglement can still be generated in other stable regions. If we try to maintain the stability of the system in all detuning range, the detuning deviation $\Delta_d = 2\pi \times 4$ kHz can meet our needs, as shown in Figure 5(b). Beyond the near-zero region, systems operating at different detuning points have different sensitivities to detuning deviations. As shown in Figures 5(c) and 5(d), the effective detuning of $\widetilde{9}+$ is 0.91 Δ_w and 1.1 Δ_w corresponding to $\Delta_d = -0.09\ \Delta_w$ and $0.1\,\Delta_w$, the system is still able to maintain its stability all over the detuning range. When $\Delta_d = -0.1\ \Delta_w$ and $0.11\,\Delta_w$, there would be unstable region that exists near the detuning $\Delta_w = 0$. With the absolute value of detuning deviation Δ_d increasing, the unstable region would expand. Therefore, once Δ_d exceeds about ±10 percent of Δ_w, the system will be unstable near the purple dip shown in figures and the pairwise entanglement will vanish there. Under this condition, other stable regions can still generate stable pairwise entanglement the same as mentioned above.

The influence of the damping rate of MC κ_w and input microwave power P_w on entanglement is shown in Figure 6. Intuitively, the higher damping rate of each MC may reduce the pairwise entanglement. When the input power is lower than −70 dBm, an increase in input power can enlarge the entanglement and the approximate maximum entanglement is obtained around −60 dBm, which could be realized by state-of-the-art engineering cryogenic setups [56].

As we can know from Figure 7, the wavelength of input driving laser has just a little impact on the pairwise entanglement of two microwave modes both resonate at 9 GHz. Only when the normalized optical detuning is positive, the system will reach a steady state and is capable to generate stationary microwave pairwise entanglement, and its maximum is obtained ranging from Δ_m to $2\ \Delta_m$ based on this model.

From the results shown above, we can summarize four discoveries of CV microwave pairwise entanglement based on our model. At first, as the scalability of the system

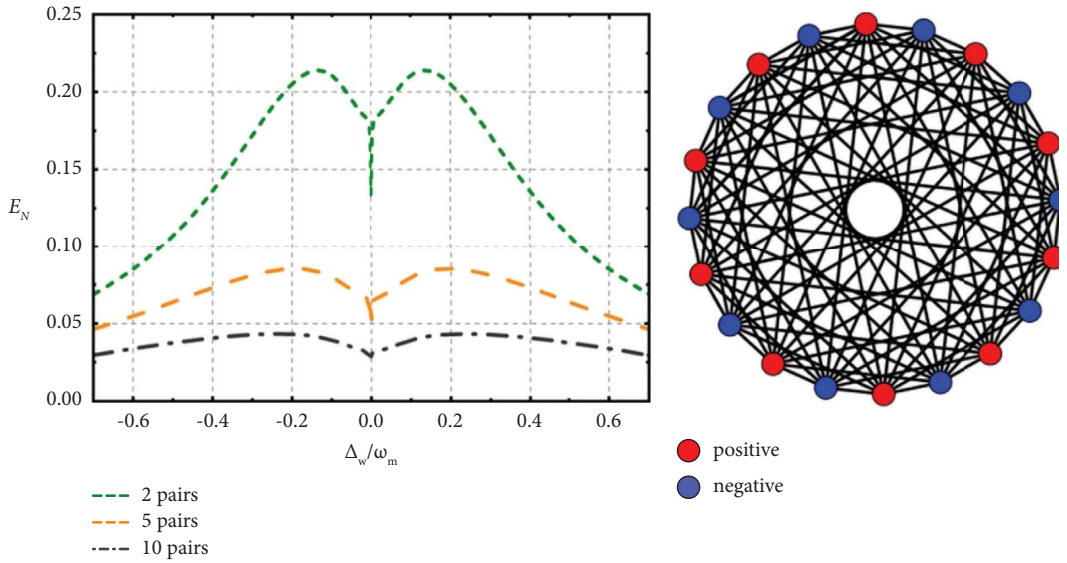

FIGURE 2: Microwave pairwise entanglement versus normalized microwave detuning Δ_w/ω_m, as the MC pair number increases. Parameters: all MC resonant frequencies are identical, $\omega_{wj} = 9$ GHz, and surrounding temperature $T = 15$ mK. The green short-dashed line shows the entanglement between two microwave modes with opposite detunings in a 2-pair system, the same is true for the orange dashed line with 5 pair MCs and the grey dot dash line with 10 pair MCs. The black line in the plot on the right shows the existence of entanglement between different MCs in the system with 10 pair MCs. "Positive" and "negative" correspond to the MCs whose effective detuning is with the same and opposite sign compared to Δ_w, respectively.

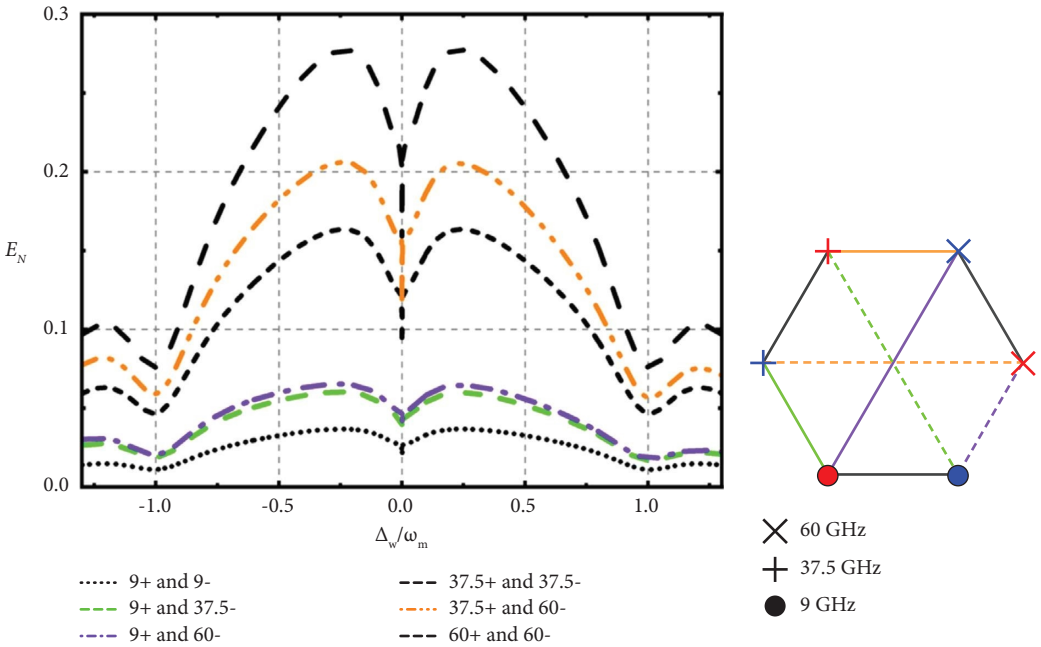

FIGURE 3: Pairwise entanglement between microwave modes with different resonant frequencies in the system containing 3-pair MCs. The first pair resonates at 9 GHz, the second at 37.5 GHz, and for the third at 60 GHz. 9+ or 9– means the MC with positive or negative detuning in the 9 GHz microwave pair, the meaning of positive or negative is the same with Figure 2, as is for 37.5± and 60±. Other parameters are the same with Figure 2.

increases, in other words, more MC pairs in the system, the microwave pairwise entanglement decreases. Secondly, higher-frequency microwave modes can get better entangled and more resistant in the thermal noise environment. Thirdly, the detunings of two entangled MCs should have opposite signs and near-absolute values. In order to reach the steady-state entanglement in all detuning range, the detuning deviation between two MCs is not supposed to exceed a particular range depending on the specific cases, for example, 10 percent in a 2-pair system. The last one, the

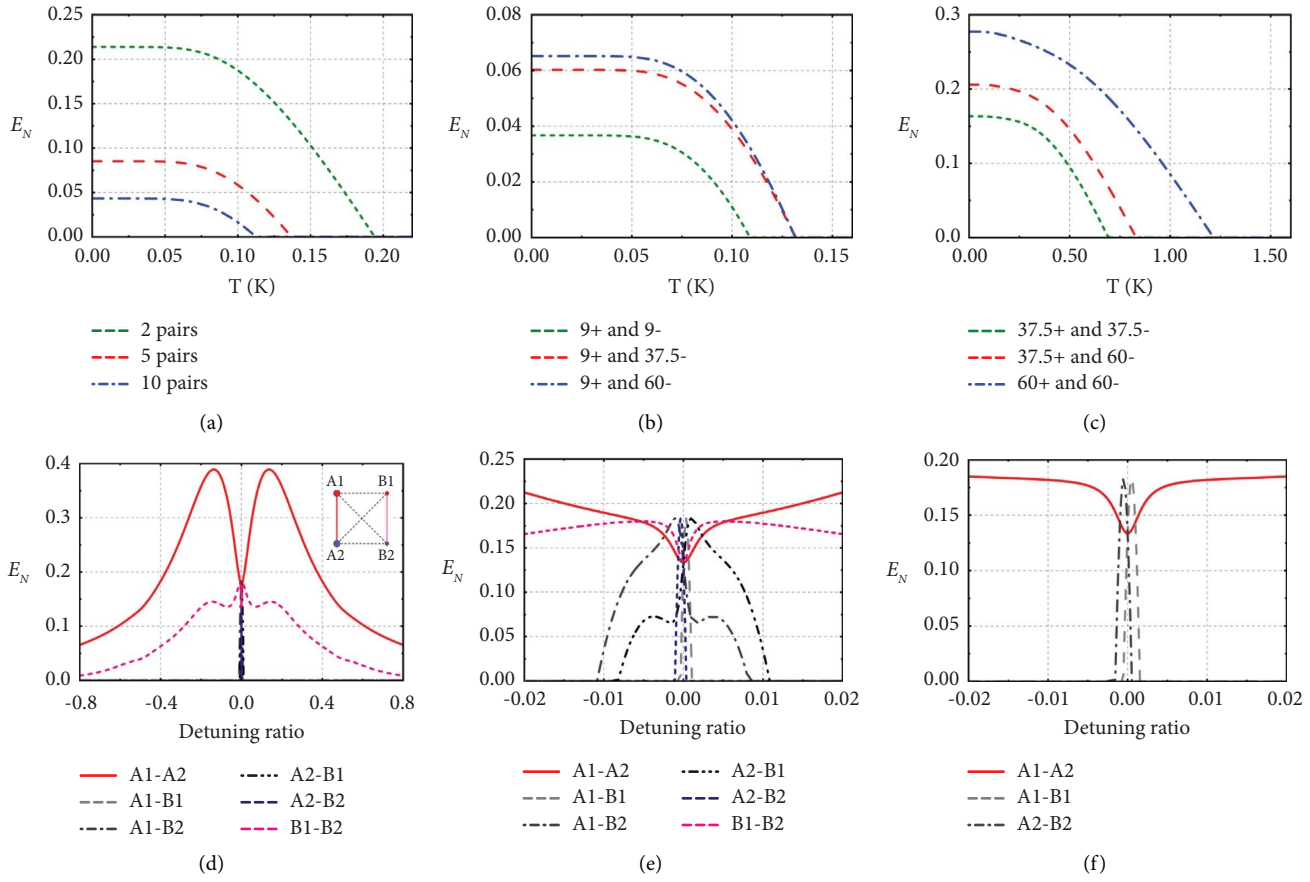

FIGURE 4: Microwave pairwise entanglement versus (a–c) temperature and (d–f) detuning ratio D_r. (a) Model described in Figure 2, with $\Delta_w = -0.14\ \omega_m$ for green short-dashed line, $\Delta_w = -0.19\ \omega_m$ for red dashed line, and $\Delta_w = -0.24\ \omega_m$ for blue dot-dashed line. (b–c) Model described in Figure 3, with $\Delta_w = -0.24\ \omega_m$ for all trace. (d–e) The effective detuning of the first MC pair $\Delta_{w1}/\omega_m = -\Delta_{w2}/\omega_m = D_r$, of the second pair $\Delta_{w3}/2\omega_m = -\Delta_{w4}/2\omega_m = D_r$. A1 indicates the MC with detuning Δ_{w1}, and A2 for the MC with detuning Δ_{w2} in the first MC pair; B1 indicates the MC with detuning Δ_{w3}, and B2 for the MC with detuning Δ_{w4} in the second MC pair. The detuning ratio D_r is ranging from −0.8 to 0.8 for (d) and from −0.02 to 0.02 for (e). (f) Model described in Figure 2 that contains 2-pair MCs; all MC shares the same detuning ratio D_r. A1-B1 and A2-B2 traces for two MCs with same absolute value and same sign. A1-A2 trace represents two MCs with the same absolute value but opposite sign. Other unmentioned parameters are the same with the 2-pair model in Figure 2.

smaller the damping rate of each MC, the better pairwise entanglement can be obtained, so does for the input power in a certain range.

Our proposal is the first report to generate CV pairwise entanglement based on the experimentally feasible parameters. As for the experimental realization, the mechanical resonator could be manifested as a parallel-plate capacitor with a moving element. The stationary plate is divided into several evenly sized sections corresponds to the number of microwave cavities, each connected to an inductor to build the capacitively electromechanical coupling with microwave cavities, while the moving plate forms an end mirror in a Fabry–Pérot cavity to interact with optical mode via radiation pressure. The interaction picture can be represented as that the optical cavity is used for driving the mechanical element motion to generate pairwise entanglement between microwave cavities. As for the comparison with other similar works, in our model the entanglement can still exceed the value of 0.2. This is on the same order of magnitude as previous theoretical work using the same measure of entanglement, allowing one to achieve higher fidelity of teleportation than can only be achieved using classical methods [24, 33–35]. We also believe that these results will be beneficial to design and control CV pairwise entanglement based on optoelectromechanical systems.

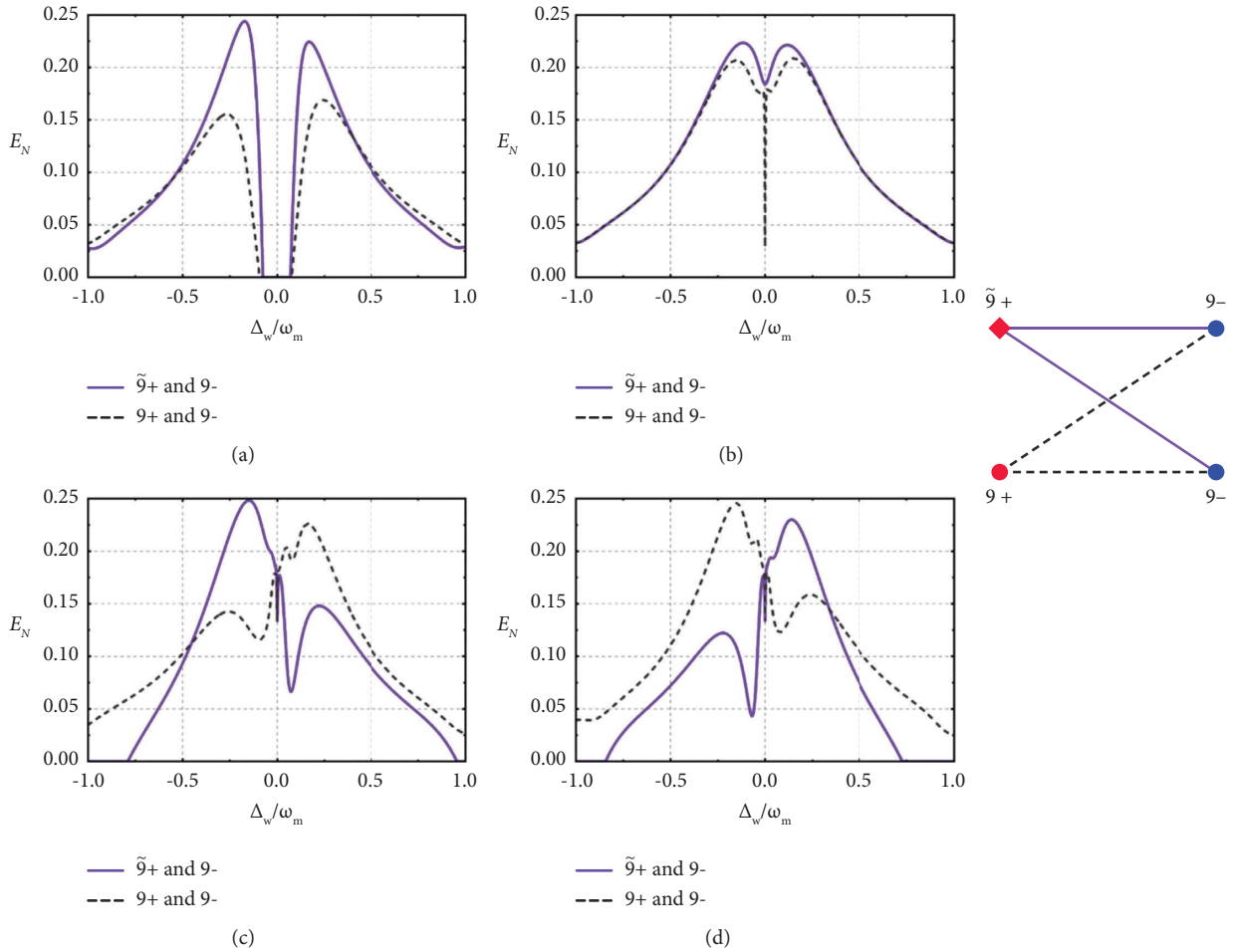

FIGURE 5: Pairwise entanglement versus normalized microwave detuning Δ_w/ω_m in a 2-pair system as detuning deviation $\Delta_d = \Delta_{w1} - \Delta_w$ of one MC changes named $\tilde{9}$+. (a) $\Delta_d = 2\pi \times 50$ kHz, (b) $\Delta_d = 2\pi \times 4$ kHz, (c) $\Delta_d = -0.09\Delta_w$, and (d) $\Delta_d = 0.1\Delta_w$. Other parameters are same with the 2-pair system in Figure 2.

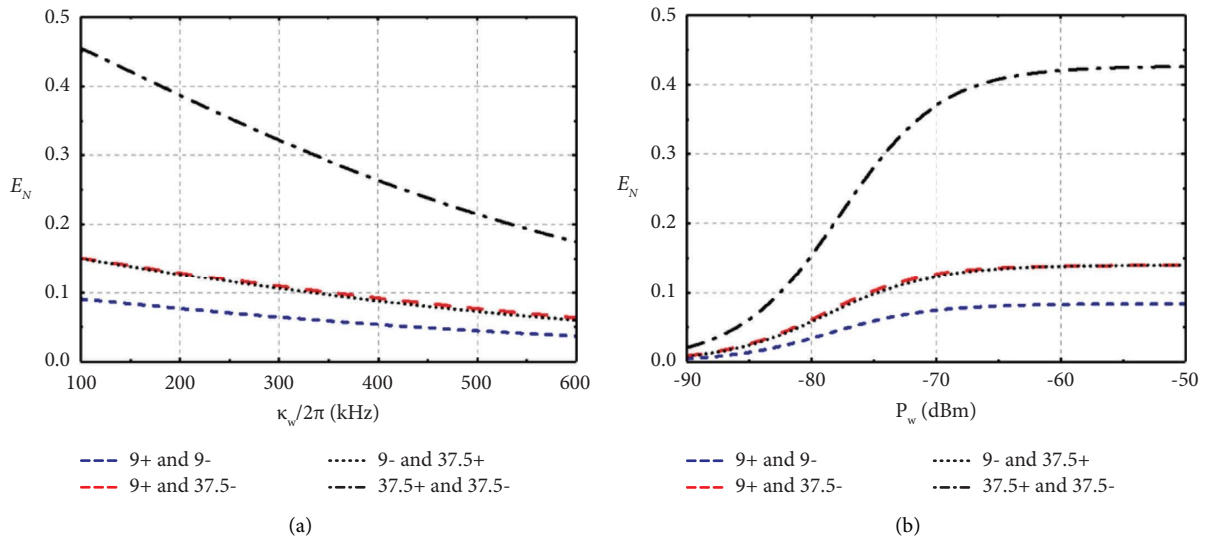

FIGURE 6: Pairwise entanglement versus (a) damping rates κ_w and (b) input power P_w in 2-pair system with resonant frequency 9 GHz for the first pair and 37.5 GHz for the second pair. Other parameters are the same with 2-pair model in Figure 2.

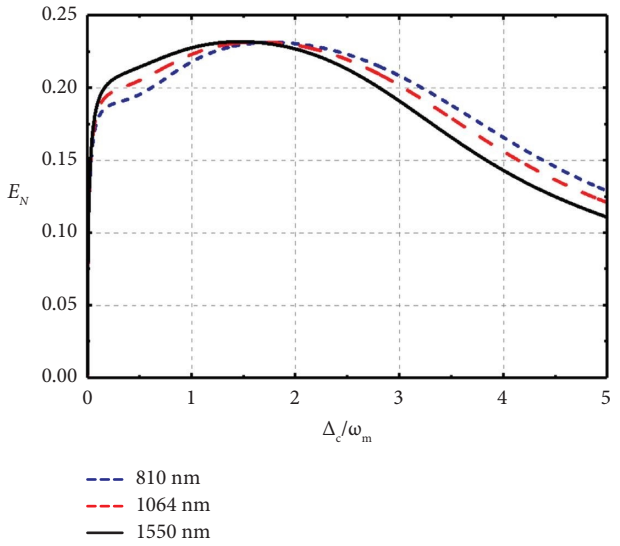

FIGURE 7: Microwave pairwise entanglement versus normalized optical detuning Δ_c/ω_m. Blue short-dashed line for driving laser with wavelength λ_{0c} = 810 nm, red dashed line for λ_{0c} = 1064 nm and black full line for λ_{0c} = 1550 nm. Other parameters are the same with 2-pair model in Figure 2.

5. Conclusion and Outlook

In conclusion, we have studied the CV microwave pairwise entanglement based on a hybrid optoelectromechanical system. We have analyzed the influence of several key parameters, such as the MC pair number, microwave resonant frequency, ambient temperature, and detuning deviation of each MC, on CV pairwise entanglement. Such a model may play important role in various rapid-developing quantum technologies with the trend that the platforms of quantum technologies are getting increasingly scalable and integrated, like quantum Internet [1–3] and quantum short-range radars [39–41]. For example, the prototype microwave quantum illumination radar described in reference [41] uses two entangled microwave radiation (one pair) to enhance the performance of detecting a 1 m apart target, in which the signal mode is used to detect targets and the idler mode is reserved locally waiting for the returned signal for homodyne measurement. However, if we want to detect targets from all directions at the same time, one pair of microwave modes may not enough, and the effect of the traditional radar's rotating scanning method on such a quantum system is still not thoroughly studied. Our model can simultaneously generate multiple pairs of entangled microwave modes that can obtain multiple sets of parallel data of targets, which has the potential to solve this problem. Besides, our model could be further used to the case that multiple pairs of optical modes simultaneously pump and resonant in the optical cavity. In this condition, the multiple pairs of microwave-optical pairwise entanglement with broadband can be generated, which has wide-ranging implications in hybrid quantum networks in the context of communication, sensing, and computing.

Appendix

A. Drift Matrix and Calculation of Logarithmic Negativity

The explicit expression of drift matrix A is

$$A = \begin{pmatrix} 0 & \omega_m & 0 & 0 & 0 & 0 & 0 & 0 & \dots, & 0 & 0 & 0 & 0 \\ -\omega_m & k_m & G_c & 0 & G_{w1} & 0 & G_{w2} & 0 & \dots, & G_{w(n-1)} & 0 & G_{wn} & 0 \\ 0 & 0 & -k_c & \Delta_c & 0 & 0 & 0 & 0 & \dots, & 0 & 0 & 0 & 0 \\ G_c & 0 & -\Delta_c & -k_c & 0 & 0 & 0 & 0 & \dots, & 0 & 0 & 0 & 0 \\ 0 & 0 & 0 & 0 & -k_{w1} & \Delta_{w1} & 0 & 0 & \dots, & 0 & 0 & 0 & 0 \\ G_{w1} & 0 & 0 & 0 & -\Delta_{w1} & -k_{w1} & 0 & 0 & \dots, & 0 & 0 & 0 & 0 \\ 0 & 0 & 0 & 0 & 0 & 0 & -k_{w2} & \Delta_{w2} & \dots, & 0 & 0 & 0 & 0 \\ G_{w2} & 0 & 0 & 0 & 0 & 0 & -\Delta_{w2} & -k_{w2} & \dots, & 0 & 0 & 0 & 0 \\ \dots, & \dots, & \dots, & \dots, & \dots, & \dots, & \dots, & \dots, & \dots, & \dots, & \dots, & \dots, & \dots, \\ 0 & 0 & 0 & 0 & 0 & 0 & 0 & 0 & \dots, & -k_{w(n-1)} & \Delta_{w(n-1)} & 0 & 0 \\ G_{w(n-1)} & 0 & 0 & 0 & 0 & 0 & 0 & 0 & \dots, & -\Delta_{w(n-1)} & -k_{w(n-1)} & 0 & 0 \\ 0 & 0 & 0 & 0 & 0 & 0 & 0 & 0 & \dots, & 0 & 0 & -k_{wn} & \Delta_{wn}, \\ G_{wn} & 0 & 0 & 0 & 0 & 0 & 0 & 0 & \dots, & 0 & 0 & -\Delta_{wn} & -k_{wn}. \end{pmatrix}. \quad \text{(A.1)}$$

If the real part of all the eigenvalues of the drift matrix \$A\$ is negative, the system is stable and will approach a steady state. The exact calculation by Routh–Hurwitz theorem is too cumbersome so we omit them here, and the solution of equation (12) is

$$u(t) = M(t)u(0) + \int_0^t ds\, M(s)n(s), \tag{A.2}$$

where $M(t) = \exp\ (\mathrm{At})$ and $n(t)$ is the noise vector.

The steady state of the system's quantum fluctuations is completely characterized by the $n \times n$ correlation matrix with its components $V_{ij} = u_i(\infty)u_j(\infty) + u_j(\infty)u_i(\infty)/2$, When the system is stable, the components become

$$V = \int_0^\infty ds\, M(s)\mathrm{DM}^T(s), \tag{A.3}$$

and $M(\infty) = 0$. With the help of Lyapunov's first theorem, equation (A.3) is equivalent to equation (13): $\mathrm{AV} + \mathrm{VA}^T = -D$.

Data Availability

The data that support the findings of this study are available from the corresponding author upon reasonable request.

Disclosure

An arXiv has previously been published [57].

Conflicts of Interest

The authors declare that they have no conflicts of interest.

Acknowledgments

This work was supported by the National Key Research and Development Program of China (Grant nos. 2018YFA0307400 and 2018YFA0306102), Sichuan Science and Technology Program (Grant nos. 2021YFSY0063, 2021YFSY0062, 2021YFSY0064, 2021YFSY0065, 2021YFSY0066, 2022YFSY0061, 2022YFSY0062, and 2022YFSY0063), National Natural Science Foundation of China (Grant nos.U19A2076 and 62005039), and Innovation Program for Quantum Science and Technology (Grant no. 2021ZD0301702).

References

[1] H. Kimble, "The quantum internet," *Nature*, vol. 453, no. 7198, pp. 1023–1030, 2008.

[2] S. Wehner, D. Elkouss, and R. Hanson, "Quantum internet: a vision for the road ahead," *Science*, vol. 362, no. 6412, 2018.

[3] S. Pirandola and S. Braunstein, "Physics: unite to build a quantum internet," *Nature*, vol. 532, no. 7598, pp. 169–171, 2016.

[4] F. Arute, K. Arya, R. Babbush et al., "Quantum supremacy using a programmable superconducting processor," *Nature*, vol. 574, no. 7779, pp. 505–510, 2019.

[5] T. Ladd, F. Jelezko, R. Laflamme, Y. Nakamura, C. Monroe, and J. O'Brien, "Quantum computers," *Nature*, vol. 464, no. 7285, pp. 45–53, 2010.

[6] N. Gisin and R. Thew, "Quantum communication," *Nature Photonics*, vol. 1, no. 3, pp. 165–171, 2007.

[7] C. Degen, F. Reinhard, and P. Cappellaro, "Quantum sensing," *Reviews of Modern Physics*, vol. 89, no. 3, Article ID 035002, 2017.

[8] S. Pirandola, B. Bardhan, T. Gehring, C. Weedbrook, and S. Lloyd, "Advances in photonic quantum sensing," *Nature Photonics*, vol. 12, pp. 724–733, 2018.

[9] B. Nichol, R. Srinivas, D. Nadlinger et al., "An elementary quantum network of entangled optical atomic clocks," *Nature*, vol. 609, no. 7928, pp. 689–694, 2022.

[10] J. Gu, X. Cao, Y. Fu et al., "Experimental measurement-device-independent type quantum key distribution with flawed and correlated sources," *Science Bulletin*, vol. 67, no. 21, pp. 2167–2175, 2022.

[11] H. Yin, Y. Fu, C. Li et al., "Experimental quantum secure network with digital signatures and encryption," *National Science Review*, vol. 10, no. 4, 2023.

[12] Y. B. Sheng, L. Zhou, and G. Long, "One-step quantum secure direct communication," *Science Bulletin*, vol. 67, no. 4, pp. 367–374, 2022.

[13] Y. Xie, Y. Lu, C. Weng et al., "Breaking the rate-loss bound of quantum key distribution with asynchronous two-photon interference," *PRX Quantum*, vol. 3, no. 2, Article ID 020315, 2022.

[14] G. Long, D. Pan, Y. Sheng, Q. Xue, J. Lu, and L. Hanzo, "An evolutionary pathway for the quantum internet relying on secure classical repeaters," *IEEE Network*, vol. 36, no. 3, pp. 82–88, 2022.

[15] N. Lauk, N. Sinclair, S. Barzanjeh et al., "Perspectives on quantum transduction," *Quantum Science and Technology*, vol. 5, no. 2, Article ID 020501, 2020.

[16] A. Martin, J. Hlinka, and J. Davidsen, "Pairwise network information and nonlinear correlations," *Physical Review E*, vol. 94, no. 4, Article ID 040301, 2016.

[17] I. Mirza and J. Schotland, "Multiqubit entanglement in bidirectional-chiral-waveguide QED," *Physical Review A*, vol. 94, no. 1, Article ID 012302, 2016.

[18] X. Wang and K. Molmer, "Pairwise entanglement in symmetric multi-qubit systems," *European Physical Journal D: Atomic, Molecular and Optical Physics*, vol. 18, no. 3, pp. 385–391, 2002.

[19] A. Meill and D. Meyer, "Pairwise concurrence in cyclically symmetric quantum states," *Physical Review A*, vol. 100, no. 4, Article ID 042318, 2019.

[20] G. García-Pérez, M. Rossi, B. Sokolov, E. Borrelli, and S. Maniscalco, "Pairwise tomography networks for many-body quantum systems," *Physical Review Research*, vol. 2, Article ID 023393, 2020.

[21] M. Aspelmeyer, T. Kippenberg, and F. Marquardt, "Cavity optomechanics," *Reviews of Modern Physics*, vol. 86, no. 4, pp. 1391–1452, 2014.

[22] L. Midolo, A. Schliesser, and A. Fiore, "Nano-opto-electromechanical systems," *Nature Nanotechnology*, vol. 13, no. 1, pp. 11–18, 2018.

[23] J. Teufel, D. Li, M. Allman et al., "Circuit cavity electromechanics in the strong-coupling regime," *Nature*, vol. 471, no. 7337, pp. 204–208, 2011.

[24] S. Barzanjeh, D. Vitali, P. Tombesi, and G. Milburn, "Entangling optical and microwave cavity modes by means of

a nanomechanical resonator," *Physical Review A*, vol. 84, no. 4, Article ID 042342, 2011.

[25] S. Barzanjeh, M. Abdi, G. Milburn, P. Tombesi, and D. Vitali, "Reversible optical-to-microwave quantum interface," *Physical Review Letters*, vol. 109, no. 13, Article ID 130503, 2012.

[26] Q. Cai, J. Liao, and Q. Zhou, "Entangling two microwave modes via optomechanics," *Physical Review A*, vol. 100, no. 4, Article ID 042330, 2019.

[27] A. Pitanti, J. Fink, A. Safavi-Naeini et al., "Strong optoelectromechanical coupling in a silicon photonic crystal cavity," *Optics Express*, vol. 23, no. 3, pp. 3196–3208, 2015.

[28] S. Barzanjeh, E. Redchenko, M. Peruzzo et al., "Stationary entangled radiation from micromechanical motion," *Nature*, vol. 570, no. 7762, pp. 480–483, 2019.

[29] J. Bochmann, A. Vainsencher, D. Awschalom, and A. Cleland, "Nanomechanical coupling between microwave and optical photons," *Nature Physics*, vol. 9, no. 11, pp. 712–716, 2013.

[30] R. Andrews, R. Peterson, T. Purdy et al., "Bidirectional and efficient conversion between microwave and optical light," *Nature Physics*, vol. 10, no. 4, pp. 321–326, 2014.

[31] M. Forsch, R. Stockill, A. Wallucks et al., "Microwave-to-optics conversion using a mechanical oscillator in its quantum ground state," *Nature Physics*, vol. 16, no. 1, pp. 69–74, 2020.

[32] M. Abdi, P. Tombesi, and D. Vitali, "Entangling two distant non-interacting microwave modes," *Annalen der Physik*, vol. 527, no. 1-2, pp. 139–146, 2015.

[33] D. Vitali, P. Tombesi, M. Woolley, A. C. Doherty, and G. J. Milburn, "Entangling a nanomechanical resonator and a superconducting microwave cavity," *Physical Review A*, vol. 76, no. 4, Article ID 042336, 2007.

[34] C. Genes, A. Mari, P. Tombesi, and D. Vitali, "Robust entanglement of a micromechanical resonator with output optical fields," *Physical Review A*, vol. 78, no. 3, Article ID 032316, 2008.

[35] D. Vitali, S. Gigan, A. Ferreira et al., "Optomechanical entanglement between a movable mirror and a cavity field," *Physical Review Letters*, vol. 98, no. 3, Article ID 030405, 2007.

[36] C. Jiang, S. Tserkis, K. Collins, S. Onoe, Y. Li, and L. Tian, "Switchable bipartite and genuine tripartite entanglement via an optoelectromechanical interface," *Physical Review A*, vol. 101, no. 4, Article ID 042320, 2020.

[37] J. Li and S. Gröblacher, "Stationary quantum entanglement between a massive mechanical membrane and a low frequency LC circuit," *New Journal of Physics*, vol. 22, no. 6, Article ID 063041, 2020.

[38] A. Higginbotham, P. Burns, M. D. Urmey et al., "Harnessing electro-optic correlations in an efficient mechanical converter," *Nature Physics*, vol. 14, no. 10, pp. 1038–1042, 2018.

[39] S. Barzanjeh, S. Guha, C. Weedbrook, D. Vitali, J. Shapiro, and S. Pirandola, "Microwave quantum illumination," *Physical Review Letters*, vol. 114, no. 8, Article ID 080503, 2015.

[40] Q. Cai, B. Fan, Y. Fan et al., "Entangling optical and mechanical cavity modes in an optomechanical crystal nanobeam," *Physical Review A*, vol. 108, no. 2, Article ID 022419, 2023.

[41] S. Barzanjeh, S. Pirandola, D. Vitali, and J. Fink, "Microwave quantum illumination using a digital receiver," *Science Advances*, vol. 6, no. 19, 2020.

[42] U. Andersen, J. Neergaard-Nielsen, P. van Loock, and A. Furusawa, "Hybrid discrete- and continuous- variable quantum information," *Nature Physics*, vol. 11, no. 9, pp. 713–719, 2015.

[43] K. Marshall, R. Pooser, G. Siopsis, and C. Weedbrook, "Quantum simulation of quantum field theory using continuous variables," *Physical Review A*, vol. 92, no. 6, Article ID 063825, 2015.

[44] S. Lloyd and S. Braunstein, "Quantum computation over continuous variables," *Physical Review Letters*, vol. 82, no. 8, pp. 1784–1787, 1999.

[45] N. Hosseinidehaj, Z. Babar, R. Malaney, S. Ng, and L. Hanzo, "Satellite-based continuous-variable quantum communications: state-of-the-art and a predictive outlook," *IEEE Communications Surveys & Tutorials*, vol. 21, no. 1, pp. 881–919, 2019.

[46] C. Weedbrook, S. Pirandola, R. García-Patrón et al., "Gaussian quantum information," *Reviews of Modern Physics*, vol. 84, no. 2, pp. 621–669, 2012.

[47] S. Braunstein and P. van Loock, "Quantum information with continuous variables," *Reviews of Modern Physics*, vol. 77, no. 2, pp. 513–577, 2005.

[48] Q. Zhuang, J. Preskill, and L. Jiang, "Distributed quantum sensing enhanced by continuous-variable error correction," *New Journal of Physics*, vol. 22, no. 2, Article ID 022001, 2020.

[49] X. Guo, C. Breum, J. Borregaard et al., "Distributed quantum sensing in a continuous-variable entangled network," *Nature Physics*, vol. 16, no. 3, pp. 281–284, 2020.

[50] R. Benguria and M. Kac, "Quantum Langevin equation," *Physical Review Letters*, vol. 46, pp. 1–4, 1981.

[51] V. Giovannetti and D. Vitali, "Phase-noise measurement in a cavity with a movable mirror undergoing quantum Brownian motion," *Physical Review A*, vol. 63, no. 2, Article ID 023812, 2001.

[52] C. Law, "Interaction between a moving mirror and radiation pressure: a Hamiltonian formulation," *Physical Review A*, vol. 51, no. 3, pp. 2537–2541, 1995.

[53] I. Gradshteyn and I. Ryzhik, *Table of Integrals, Series and Products*, Academic, Orlando, FL, USA, 1980.

[54] G. Vidal and R. Werner, "Computable measure of entanglement," *Physical Review A*, vol. 65, no. 3, Article ID 032314, 2002.

[55] G. Adesso, A. Serafini, and F. Illuminati, "Extremal entanglement and mixedness in continuous variable systems," *Physical Review A*, vol. 70, no. 2, Article ID 022318, 2004.

[56] S. Krinner, S. Storz, P. Kurpiers et al., "Engineering cryogenic setups for 100-qubit scale superconducting circuit systems," *EPJ Quantum Technology*, vol. 6, no. 1, p. 2, 2019.

[57] Q. Cai, J. Liao, and Q. Zhou, "Continuous-variable pairwise entanglement based on optoelectromechanical system," 2020, https://arxiv.org/abs/2003.12708.